UDC 539.4

Vacuum Crack Growth Behavior of Austenitic Stainless Steel under Fatigue Loading

T. Takeda, Y. Shindo,[1] and F. Narita

Tohoku University, Sendai, Japan

[1] shindo@material.tohoku.ac.jp

УДК 539.4

Закономерности роста трещины в аустенитной нержавеющей стали при циклическом нагружении в вакууме

Т. Такеда, Я. Шиндо, Ф. Нарита

Университет Тохоку, Сендай, Япония

Описаны закономерности роста усталостных трещин в аустенитной нержавеющей стали в вакууме. С целью учета влияния среды на рост усталостных трещин проведены испытания на циклическую трещиностойкость компактных образцов на воздухе и в вакууме. Диаграммы роста усталостных трещин строили в координатах скорость роста трещины – размах J-интеграла. При этом J-интеграл рассчитывали с помощью метода конечных элементов. Для исследования механизмов распространения трещин и оценки корреляции усталостных характеристик были выполнены фрактографические исследования. Установлено, что усталостные трещины быстрее развиваются при испытаниях в воздухе, чем в вакууме, причем данный эффект зависит от асимметрии цикла.

Ключевые слова: механика разрушения, метод конечных элементов, усталостные испытания, нержавеющая сталь, скорость роста трещины, влияние среды.

Introduction. Many components of mechanical structures can be loaded in fatigue during service and consequently failure due to fatigue is of a great concern. In the conventional classification, we can distinguish three regimes as: low cycle fatigue (LCF), high cycle fatigue (HCF), and very high cycle fatigue (VHCF), i.e., failure under cyclic loading at more than 10^7 cycles. VHCF is also referred to as giga-cycle fatigue (GCF). In general, in the LCF and HCF ranges, fatigue cracks are initiated at surfaces. In the VHCF range, the internal crack nucleation occurs at stress-concentration regions, generally in the vicinity of an inclusion or a porosity [1]. However, the experimental data for the fatigue properties of structural alloys at very long lifetimes are difficult to obtain, because fatigue tests in the VHCF regime are significantly time consuming with conventional servo-hydraulic testing equipment, where a maximum loading frequency on the order of 100 Hz is typical [2].

The fatigue process consists of crack initiation and crack propagation to failure and thus, the total useful life of a cyclically loaded component is dependent upon the growth rate of cracks. In order to assess the structural integrity and useful life of components, an understanding of the fatigue crack growth characteristics of

structural alloys is essential. In the VHCF regime, cracks propagate inside the material and are isolated from the external environment. It is noteworthy that the surrounding environment is known to play a role in the fatigue crack growth behavior of engineering alloys [3, 4]. In addition, fatigue crack growth data in vacuum can be taken as the reference to examine the environmental effects. Hence, fatigue crack growth test in vacuum offers an attractive approach for investigation of the crack-tip environmental mechanisms for alloys.

In this paper, we study the fatigue crack growth behavior of an austenitic stainless steel in a vacuum environment. Fatigue crack growth tests were performed in laboratory air and vacuum to obtain the crack growth rate as a function of the *J*-integral range. The *J*-integral range was determined from an elastic-plastic finite element analysis. After conducting the fatigue crack growth tests, the associated fractographic features were examined by scanning electron microscopy (SEM).

1. **Experimental Procedure**.

1.1. ***Material and Specimen Preparation***. The commercial SUS 304 austenitic stainless steel plates were employed for the tests. The 304 alloy belongs to the class of metastable steels. The chemical composition of the as-received 304 alloy (provided by the vendor) is listed in Table 1. The Young modulus E and yield strength σ_{YS} of the 304 alloy are 191 GPa and 327 MPa, respectively. The E and σ_{YS} data were determined by tensile tests.

T a b l e 1

Chemical Composition of SUS 304 Stainless Steel (in weight percent)

C	Si	Mn	P	S	Ni	Cr
0.04	0.6	0.93	0.025	0.003	8.11	18.25

The compact tension (CT) specimens having width $W = 25$ mm and thickness $B = 5$ mm (width-to-thickness ratio $W/B = 5$), i.e., 0.2TCT specimens [5], were machined from the plates. The geometry and dimensions of the 0.2TCT specimen are shown in Fig. 1. Each specimen was fatigue-precracked in laboratory air. The precracking was continued to a nominal original crack length-to-width ratio a_0/W of 0.6. After precracking, a side-groove was made on each side of the specimens and the net specimen thickness B_N was 4 mm.

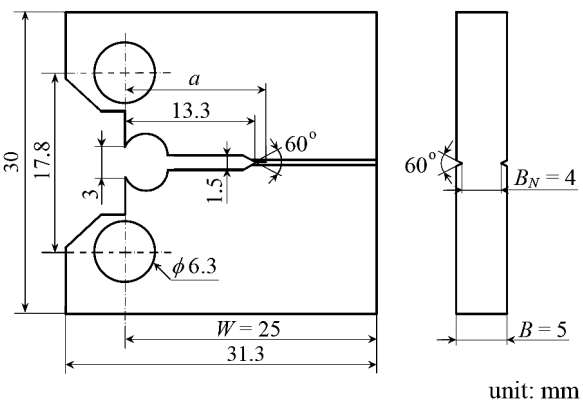

Fig. 1. Geometry and dimensions of CT specimen.

1.2. ***Fatigue Crack Growth Test and Fractography***. Fatigue crack growth tests were conducted in laboratory air and vacuum using a 30 kN capacity servohydraulic testing machine, operated under load control, with sinusoidal loading. The vacuum experiments were performed in an environmental chamber, and a turbomolecular pumping system was used to evacuate the chamber. A cyclic frequency of 3 Hz and a load ratio R of 0.1 or 0.5 were used on all tests. The load ratio R is defined as $P_{\min}/P_{\max}$, where $P_{\min}$ and $P_{\max}$ are the minimum and maximum loads applied over the fatigue cycle, respectively. The applied load was measured by the testing machine load cell. A clip gauge was used to measure the load line displacement. The instantaneous crack length a as a function of the number of cycles N was inferred from the compliance (which is the reciprocal of the load–displacement slope), and the crack growth rate da/dN was then determined.

Following the fatigue crack growth tests, the crack surface morphology was examined by SEM. Fractographs were taken for each testing environment in regions of fatigue stressing.

2. **Finite Element Analysis**. The fatigue crack growth rate da/dN can be related to the J-integral range ΔJ during fatigue loading. The J-integral range ΔJ can be obtained as $\Delta J = J_{\max} - J_{\min}$, where $J_{\max}$ and $J_{\min}$ are the maximum and minimum J-integrals corresponding to the maximum and minimum applied loads, respectively. In this study, an elastic-plastic finite element analysis was carried out for the side-grooved CT specimen of SUS 304 stainless steel in order to evaluate the J-integral range ΔJ. The commercial finite element code ANSYS was used for the analysis.

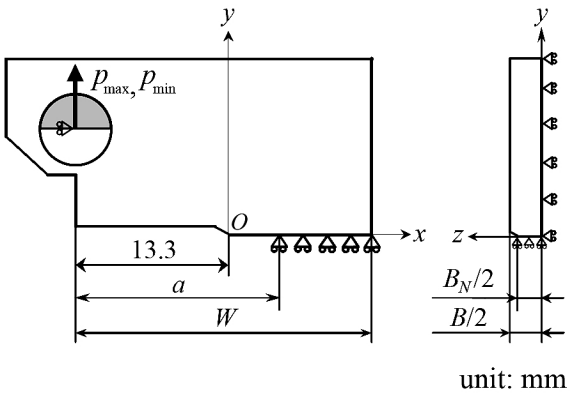

Fig. 2. Illustration of boundary conditions on the CT specimen model.

The finite element model of the side-grooved CT specimen was three-dimensional, and the CT specimen was modeled and loaded, as shown in Fig. 2, where $Oxyz$ is the Cartesian coordinate system. Owing to symmetry, only one quarter of the specimen needs to be analyzed. The finite element model of the CT specimen was based on the geometry and dimensions of the specimen. A mechanical load was produced by the application of the uniformly distributed load per unit thickness $p_{\max}$, $p_{\min}$. The uniformly distributed loads, $p_{\max}$ and $p_{\min}$, correspond respectively to the maximum and minimum applied loads as read by a load cell in the experiments. The incremental plasticity theory and the von Mises

yield criterion were employed. Let the uniaxial stress σ – strain ε curve be fitted by the following relationships:

$$\sigma = \begin{cases} E\varepsilon, & \text{for} \quad \varepsilon \le \varepsilon_{YS}, \\ \alpha\varepsilon^{A}, & \text{for} \quad \varepsilon \ge \varepsilon_{YS}, \end{cases} \tag{1}$$

where $\varepsilon_{YS} = \sigma_{YS}/E$ is the yield strain, α is a constant, and A is the strain hardening exponent. The values of α and A can be determined based on the experimental stress-strain behavior. For SUS 304 stainless steel, we obtained $\alpha = 1140$ MPa and $A = 0.2$ from the tensile test data.

The *J*-integrals at the mid-thickness of the CT specimen ($z = 0$) were used to obtain the *J*-integral range ΔJ. The *J*-integral at $z = 0$ is given by

$$J = \int_{\Gamma_0} \left\{ wn_x - \left(\sigma_{xx} \frac{\partial u}{\partial x} + \sigma_{xy} \frac{\partial u_y}{\partial x} \right) n_x - \left(\sigma_{xy} \frac{\partial u_x}{\partial x} + \sigma_{yy} \frac{\partial u_y}{\partial x} \right) n_y \right\} d\Gamma, \tag{2}$$

where Γ_0 is a contour enclosing a crack tip, w is the strain energy density, σ_{xx}, σ_{yy}, and σ_{xy} are the components of the stress tensor, u_x and u_y are the components of the displacement vector, and n_x and n_y are the components of the outer unit normal vector.

3. **Results and Discussion**. The amounts of crack extension Δa, i.e., the lengths of fatigue crack measured from the initial crack tip ($\Delta a = a - a_0$), in air and vacuum as a function of the number of cycles N are shown in Fig. 3 under the maximum applied load $P_{\max} = 2.0$ kN at the load ratio $R = 0.1$. The amount of crack extension increases with the increase in the number of cycles. Also, the crack extension amount in air is slightly larger than that in vacuum. Figure 4 shows the plots of the crack extension amount Δa versus number of cycles N at the load ratio $R = 0.5$. At $R = 0.5$, with increasing fatigue cycles the crack growth in air accelerates more rapidly than in vacuum.

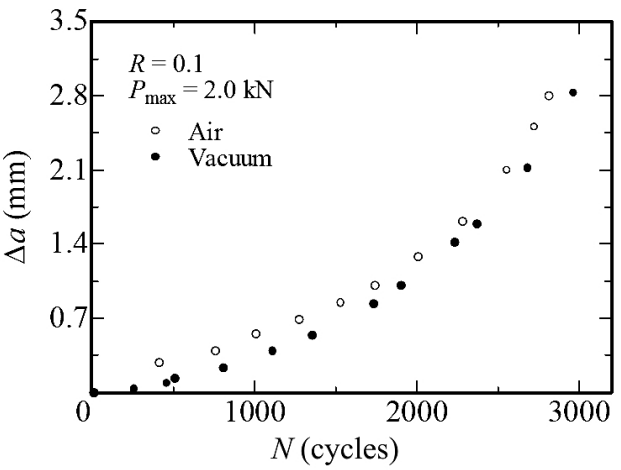

Fig. 3. The amount of crack extension Δa versus the number of cycles N at the load ratio $R = 0.1$.

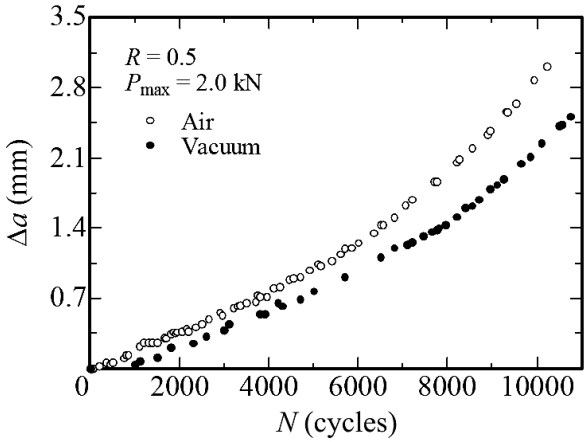

Fig. 4. The amount of crack extension Δa versus the number of cycles N at the load ratio $R = 0.5$.

The fatigue crack growth behavior in air and vacuum at the load ratio $R = 0.1$ is shown in the form of crack growth rate da/dN as a function of J-integral range ΔJ, in Fig. 5. Although the da/dN versus ΔJ data exhibit some scatter, the crack growth rate in air is higher than that in vacuum at lower ΔJ. In contrast, at higher ΔJ the da/dN versus ΔJ curves for the tests in air and vacuum nearly overlap. The trend in the fatigue crack growth behavior can be explained with the mechanisms of environmentally assisted damage at the crack tip. The acceleration of the crack growth rate in air can be attributed to the adsorption of gaseous species by the freshly exposed bare metal at the crack tip [6]. At lower ΔJ, where the crack is growing slowly, there is enough time for the gaseous species to adsorb onto the freshly exposed metal surface at the crack tip. As a result the air environment accelerates the damage process. When the crack is growing faster at higher ΔJ, adsorption rates are slower than the rate of crack advance, resulting in lesser crack-tip environmental damage. The fatigue crack growth results at the load ratio $R = 0.5$ are plotted in Fig. 6. The figure clearly shows an accelerated crack growth in air compared to that in vacuum.

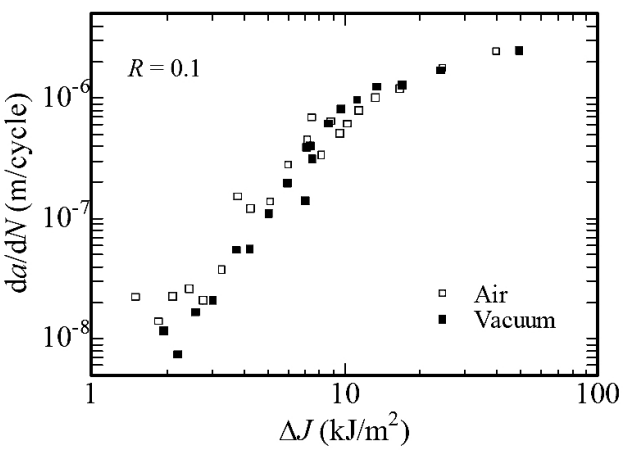

Fig. 5. Fatigue crack growth rate da/dN versus J-integral range ΔJ at the load ratio $R = 0.1$.

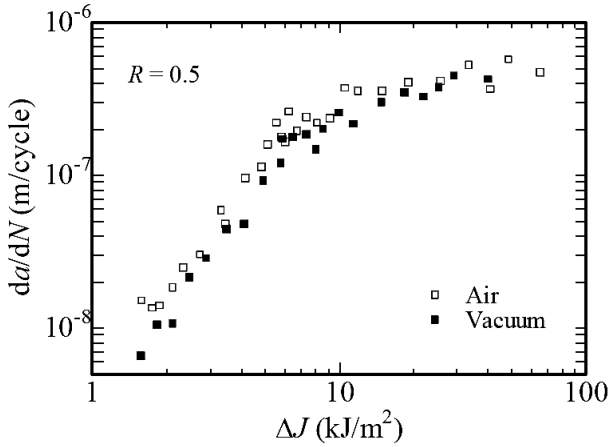

Fig. 6. Fatigue crack growth rate da/dN versus J-integral range ΔJ at the load ratio $R = 0.5$.

The SEM micrographs of the fracture surfaces in air and vacuum at the load ratio $R = 0.5$ for high ΔJ levels are shown in Fig. 7, where the direction of crack propagation is from top to bottom. Although the fracture surfaces display ductile dimple features and some transgranular cleavages, the micrographs reveal the fractographic difference in air and vacuum. That is, the SUS 304 specimens show a more cleavage morphology in air. The fracture surfaces in air and vacuum at the load ratio $R = 0.1$ for high ΔJ levels also show the ductile dimple fracture, however, the test environment does not considerably affect the fractographic features (not shown). The above fatigue crack morphology changes correlate with the trends of the crack growth behavior. The SEM micrographs of the fracture surfaces in air and vacuum at the load ratio $R = 0.5$ for low ΔJ levels are shown in Fig. 8. For low ΔJ levels, the fracture surfaces are smooth and consist of predominately transgranular cleavages. Also, clear fractographic differences in air and vacuum are not seen in the SEM images. Similar characteristics are observed for the fracture surfaces at the load ratio $R = 0.1$ for low ΔJ levels (not shown).

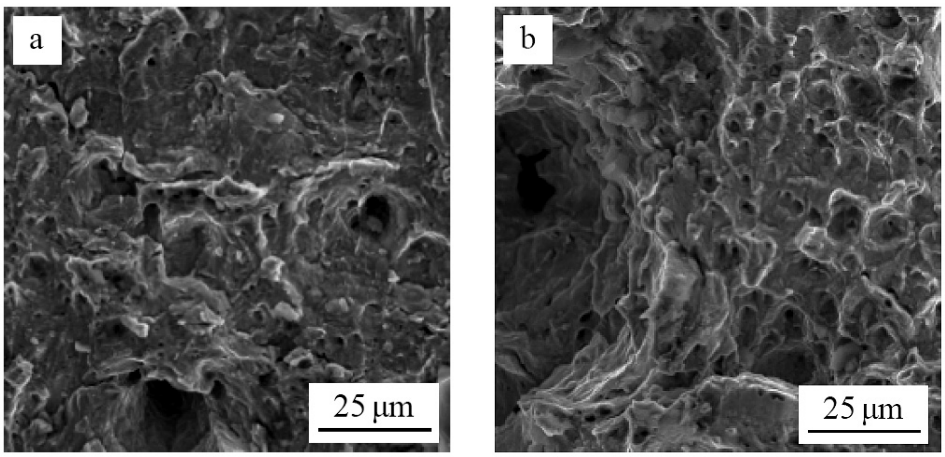

Fig. 7. SEM observations of the fracture surfaces at the load ratio $R = 0.5$ for high ΔJ levels: (a) air; (b) vacuum (crack propagation from top to bottom).

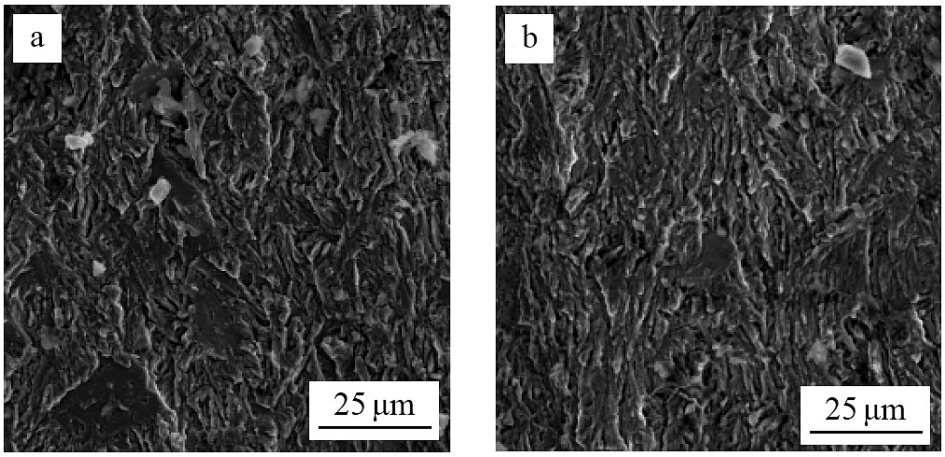

Fig. 8. SEM observations of the fracture surfaces at the load ratio $R = 0.5$ for low ΔJ levels: (a) air; (b) vacuum (crack propagation from top to bottom).

Conclusions. The focus of this paper is the study of the fatigue crack growth behavior of an austenitic stainless steel in a vacuum environment. It is found that the exposure to laboratory air increases the rate of fatigue crack propagation. Also, this environmental effect is shown to be dependent on the load ratio R. At $R = 0.5$, the fatigue crack growth rates are clearly higher in air than in vacuum. On the other hand, the crack growth rates in air merge with vacuum results as J-integral range increases at $R = 0.1$. Such a trend can be related to the crack-tip mechanisms of environmentally assisted damage. In addition, the changes in fatigue crack growth behavior are accompanied by the fracture morphology changes.

Р е з ю м е

Описано закономірності росту тріщин втомленості в аустенітній нержавіючій сталі у вакуумі. Із метою врахування впливу середовища на ріст тріщин втомленості проведено випробування на циклічну тріщиностійкість компактних зразків у повітрі і вакуумі. Діаграми росту тріщин втомленості будували в координатах швидкість росту тріщини – розмах J-інтеграла. При цьому J-інтеграл розраховували за допомогою методу скінченних елементів. Для дослідження механізмів поширення тріщин і оцінки кореляції характеристик утоми проведено фрактографічні дослідження. Установлено, що тріщини втомленості швидше поширюються при випробуваннях у повітрі, ніж у вакуумі, причому даний ефект залежить від асиметрії циклу.

1. K. Shiozawa and L. Lu, “Internal fatigue failure mechanism of high strength steels in gigacycle regime,” *Key Eng. Mater*., **378-379**, 65–80 (2008).
2. J. Z. Yi, C. J. Torbet, Q. Feng, et al., “Ultrasonic fatigue of a single crystal Ni-base superalloy at 1000°C,” *Mater. Sci. Eng. A*, **443**, 142–149 (2007).
3. M. H. Kelestemur and T. K. Chaki, “The effect of various atmospheres on the threshold fatigue crack growth behavior of AISI 304 stainless steel,” *Int. J. Fatigue*, **23**, 169–174 (2001).

4. K. Sadananda and A. K. Vasudevan, "Fatigue crack growth mechanisms in steels," *Ibid*, **25**, 899–914 (2003).
5. Y. Shindo, T. Takeda, M. Suzuki, and F. Narita, "Fatigue crack growth behavior of metastable austenitic stainless steel in cryogenic high magnetic field environments," *Metall. Mater. Trans. A*, **40**, No. 8, 1863–1867 (2009).
6. A. J. McEvily, J. L. Gonzalez, and J. M. Hallen, "Dislocation substructures at fatigue crack tips of 304 stainless steel cycled in air or vacuum," *Scripta Mater*., **35**, No. 6, 761–765 (1996).

Received 08. 06. 2010